Reaction of NH ($X\ ^3\Sigma^-$) with NO in Xenon Matrix: Infrared Detection of the HNNO Intermediate†

Sandra L. Laursen,* Alice E. Delia, and Kwasi Mitchell

Department of Chemistry, Kalamazoo College, Kalamazoo, Michigan 49006

Received: October 29, 1999; In Final Form: January 10, 2000

The reaction of ground-state NH with NO has been investigated in solid xenon matrix. NH radicals are formed in good yield in Xe matrix after UV photolysis of HN_3 and are reacted with NO in the matrix by annealing the solid to 40 K. A photolabile product is formed and identified as *trans*-HNNO by infrared spectroscopy, including isotope labeling and comparison with published frequencies from quantum chemical calculations. A minor product with similar formation and photodestruction behavior is assigned to the *cis*-HNNO isomer. Cis−trans interconversion was also observed. The reaction to form HNNO is essentially activationless. Upon photolysis at wavelengths up to 600 nm, HNNO is destroyed and converted to N_2O. This is the first detection of this intermediate, which plays a role in ammonia combustion and NO_x removal schemes.

Introduction

The radical−radical reaction between NH and NO is of substantial pragmatic interest because of its importance in combustion of nitrogenous fuels such as ammonia, hydrazine, and nitramine propellants.[1,2] It influences the level of nitrogen oxide (NO_x) emissions from these systems and plays a role in the Thermal DeNOx and RAPRENOx schemes to reduce NO_x emissions from flue gases by reaction with ammonia.[1,3]

The reaction of NH with NO has been examined using several experimental and theoretical approaches. Rate constant measurements have been reported by several groups.[4−9] The case of NH + NO contrasts with most NH reactions, for which the reaction rate for the NH (a $^1\Delta$) state is substantially faster than the reaction rate from the NH ($X\ ^3\Sigma^-$) state. The reaction NH (X) + NO has a room-temperature rate coefficient near 5×10^{-11} cm^3 molecule^{-1} s^{-1}, while the NH (a) + NO rate coefficient is about half that value. These reactions are both rapid compared with NH reaction with nonradical reactants.

Product studies have also been reported for this reaction, using both ground-state and electronically excited NH as the reactant. Though some earlier authors drew contrary conclusions,[4,10] recent product studies approach consensus that the major product on the ground-state surface is H + N_2O, accounting for 70−80% of the products at a wide range of temperatures.[8,11−16] The other exothermic reaction channel, OH + N_2, accounts for the rest. Though the OH + N_2 product channel is more exothermic, the lower barrier and looser transition state to H + N_2O are thought to govern product distribution. For the excited NH (a) state, electronic quenching is the major removal path (ca. 50%), with the H + N_2O and OH + N_2 channels nearly equal in importance among the chemical channels and a minor O (^{3}P) + N_2H channel becoming energetically accessible.[6,8]

For both NH (a) and NH (X) reaction with NO, activationless formation of an HNNO intermediate is postulated as the first and rate-limiting step in the reaction. Several pieces of experimental evidence point to the existence of a bound intermediate. The rate coefficient is temperature-independent at ordinary temperatures.[4,13,17] A crossed-beam study of NH (X) + NO found λ-doublet preferences in the OH rotational distribution, indicating that a planar intermediate is the precursor to OH.[18] Evidence for a long-lived HNNO intermediate is also seen in studies of the reverse reaction, H + N_2O, under a variety of conditions.[19−21] In the gas phase, the intermediate fragments faster than it can be stabilized, accounting for the lack of observed pressure dependence of the rate coefficient.[22] Finally, HNNO has been suggested to be an intermediate in the reaction of O + NNH, a reaction that may contribute to NO_x production in flames.[23,24]

In addition to the experimental work, several theoretical studies have examined the energetics and dynamics for the HNNO system.[11,15,19,25−29] The studies agree on the general shape of the PES, including a bound minimum for HNNO, and locate the barrier from HNNO to H + N_2O at a lower energy than that to OH + N_2. RRKM calculations based on high-quality ab initio energies[15,25] reproduce the experimental rate constants and product branching ratios reasonably well.[26−28] The studies also concur that an activationless route to HNNO exists for both singlet and triplet NH reactions, when surface crossings are taken into account, and that HNNO is bound by some 250 kJ mol^{-1} relative to ground-state NH + NO.[11,15,25,27]

In this study, we examine the reaction

$$\mathrm{NH}\ (X\ ^3\Sigma^-) + \mathrm{NO}\ (X\ ^2\Pi) \rightarrow \mathrm{HNNO}\ (\tilde{X}\ ^2A') \qquad (1)$$

using matrix isolation techniques. NH is prepared in its electronic ground state by UV photolysis of HN_3 in a solid xenon matrix. The heavy-atom matrix induces rapid intersystem crossing of the initially formed NH (a $^1\Delta$) state to yield NH ($X\ ^3\Sigma^-$) trapped in the solid at 11 K. Annealing of the matrix to 40 K softens the matrix sufficiently to permit diffusion and reaction with co-trapped NO. HNNO is identified as the product by its infrared spectrum and subsequent photochemical depletion behavior. This is the first direct observation of this species.

Experimental Method

The experimental apparatus has been described in detail previously.[30] Briefly, gaseous mixtures of HN_3/NO/Xe at concentrations near 2:1:400 were deposited at 0.5−1 mmol h^{-1}.

† Part of the special issue "Marilyn Jacox Festschrift".

* Corresponding author. Present address: NOAA Aeronomy Lab, R/AL2, 325 Broadway, Boulder, CO 80303. E-mail: SLaursen@AL.noaa.gov.

10.1021/jp993854i CCC: $19.00
Published on Web 02/29/2000

Hydrazoic acid was generated by reaction of NaN_3 and molten octadecanoic acid under vacuum at about 95 °C, keeping pressures below 5 Torr to reduce the explosion hazard. Nitric oxide (99.5%, AGA) was purified by evaporation from a 77 K condensate. Some N_2O and NO_2 impurities were still observed after preparing the matrix and may have formed in the bulb or during deposition. Labeled ^{15}NO (ICON Stable Isotopes, 99% N-15) and Xe (99.995%, AGA) were used as received.

The xenon mixtures were deposited at 28−35 K onto a CsI substrate mounted on a rotatable cold head cooled by an APD HC-202 helium refrigerator. FTIR spectra (100 scans, 400−4000 cm^{-1}) were collected at 11 K through CsI windows, using a dry air-purged Nicolet Magna-IR 550 spectrometer at 0.5 cm^{-1} resolution. To generate NH via photodissociation of HN_3, matrices were irradiated through a fused silica window at 254 nm (∼20 nm fwhm) using a PTI 200-W Hg/Xe lamp and 0.25 m monochromator. In typical samples, 2 h of photolysis were sufficient to deplete the HN_3 absorptions by 95% or more. Samples were slowly annealed to 40−44 K to allow diffusion of reactants, then recooled to 11 K for further study. Subsequent long-wavelength photolyses (700−300 nm, as noted) of the products were conducted using the Hg/Xe lamp and monochromator system, using filters to remove higher order radiation.

Results

A complete list of the infrared frequencies, intensities, intensity changes, and band assignments for these experiments is available as Table S1 in the Supporting Information. Infrared absorptions observed in HN_3/NO/Xe 2:1:400 matrices are assigned to isolated HN_3 (bands near 3298, 2133, 1263, 1145, 535 cm^{-1}) and higher multimers,[30] isolated NO, and NO dimers. The NO monomer and dimer absorptions are assigned by comparison with our own studies of NO/Xe matrices, including ^{15}N isotope studies, and with literature spectra of NO aggregates in Ne, Ar, and N_2 matrixes.[31−33] Isolated NO is seen at 1866.6 cm^{-1} and NO dimer bands near 1854 and 1745 cm^{-1}, which we have assigned to the more stable *cis*-$(NO)_2$ species. The absorptions of NO_2 and N_2O impurities in the NO samples are also identified, in multiple matrix sites.[34,35]

Upon photolysis at 254 nm, the HN_3 absorptions diminish substantially and new features grow in. These changes are shown in traces a of Figures 1 and 2. The most prominent of these are a set of absorptions at 3131.8, 3120.6, and 3109.0 cm^{-1} previously assigned to NH in Xe matrix based on literature reports and studies of HN_3/Xe matrices.[30] This splitting of the vibrational fundamental does not match the rotational structure for NH in Xe[36−38] and is ascribed to site splittings. The nitrogen cage partner is present nearby in the cage and may hinder rotation.[39] Weak bands assigned to HONO[31,40] and NH_2OH[41] can also be detected at this stage.[30] The relative intensities of the dimer and monomer bands of NO change during photolysis, with the monomer bands growing and the dimer bands decreasing. NO_2 and N_2O bands increase in intensity during photolysis as well. These latter changes also occur upon 254 nm photolysis of NO/Xe matrices with HN_3 absent.

In studies of HN_3/Xe matrices with no NO present, NH was the only photolysis product detected. This is consistent with literature reports that NH is the predominant product of HN_3 photolysis in this energy regime.[42] Although the H + N_3 channel is energetically accessible at 254 nm and has been reported as a minor photodissociation channel,[43,44] no evidence was seen for formation of N_3, the infrared spectrum of which is known.[31] Cage recombination of the ground-state radicals H + N_3 may be rapid, whereas for NH + N_2 cage recombination is not spin-allowed once the NH has undergone intersystem crossing. We thus assume that the quantum yield of trapped H atoms is low and that NH is the principal reactive species trapped in the matrix after HN_3 photolysis. Because the infrared spectrum is taken long after photolysis, relative to the NH ($a\ ^1\Delta$) relaxation time in Xe,[39] there is no question that the NH trapped in the matrix and observed by IR is electronically and internally cold NH in its ($X\ ^3\Sigma^-$) ground state.

When photolyzed samples are annealed to 40 K, the NH bands at 3132, 3120, and 3109 cm^{-1} diminish in intensity and several new features appear. These changes are displayed in traces b of Figures 1 and 2. In order of intensity, these include doublets at 1628.9/1627.1, 1213.4/1214.7, and 1294.5/1296.2 cm^{-1}, singlets at 3254.0 and 746.5 cm^{-1}, and doublets at 2908.7/2911.6 and 2826.5/2825.1 cm^{-1}. The frequencies and relative intensities of these features are included in Table 1. Growth and depletion behavior, presented in Figure 3 and discussed in more detail below, allows us to identify these bands as representing a common molecular species, hereafter referred to as I. In experiments in which the I bands were most intense, a second set of bands is also observed. These are found at 1621.4/1623.7/1622.3, 1166.9, 1273.4, 3158, and 712.1 cm^{-1}, and are listed in Table 2. Their growth and loss behavior (represented in Figure 3) suggests that together they represent a second species II. Each of these bands lies close to one of the stronger type I bands, within 3−4% in wavenumber. Their intensities relative to the type I bands varied. For accuracy, the relative intensities in Table 2 are derived from the experiment in which they were most prominent, in which the strongest band of II had an absorbance 66% of that of the strongest band of I. The spectra in Figures 1 and 2 show lower and more typical intensities for the type II bands. Some studies at differing ratios of HN_3 and/or NO were performed; product yields were lower, but type I bands could still be observed. Although the concentrations used in these experiments (ca. 2:1:400) are high for purely spectroscopic studies, they are comparable to matrix compositions found effective in other studies of bimolecular reactions in matrices.

Infrared absorptions of HNOO[30] formed from reaction of NH ($X\ ^3\Sigma^-$) with oxygen impurities could sometimes be observed in these samples as well. Finally, the NO monomer absorption decreased in intensity and the NO dimer absorptions increased in intensity, a process which also occurred in NO/Xe samples without HN_3. Changes in NO_2 and N_2O absorptions are complex but are likewise observed in NO/Xe samples with no HN_3 present. Traces d in Figures 1 and 2 show the infrared spectrum for an NO/Xe sample in the spectral regions where the bands of I and II appeared. This NO/Xe sample was prepared and treated the same as samples that yielded the I and II bands, by 254 nm photolysis then annealing, except that HN_3 was omitted from the matrix.

When samples previously photolyzed and annealed are irradiated at long wavelengths, both sets of absorptions I and II disappear. Irradiation at wavelengths in the range 500−600 nm depletes both slowly, while photolysis at wavelengths ≤400 nm causes more rapid depletion. The effect of 550 nm radiation is shown in traces c of Figures 1 and 2; the "mirror image" appearance of traces b and c is an identifying characteristic common to both sets of bands I and II. However, irradiation at 700 nm depletes the type II bands and causes the type I bands to increase, a key distinguishing feature of the two sets. Loss of type II bands and growth of type I bands was also seen in samples allowed to stand overnight at 11 K after annealing. These samples were rotated out of the IR spectrometer beam

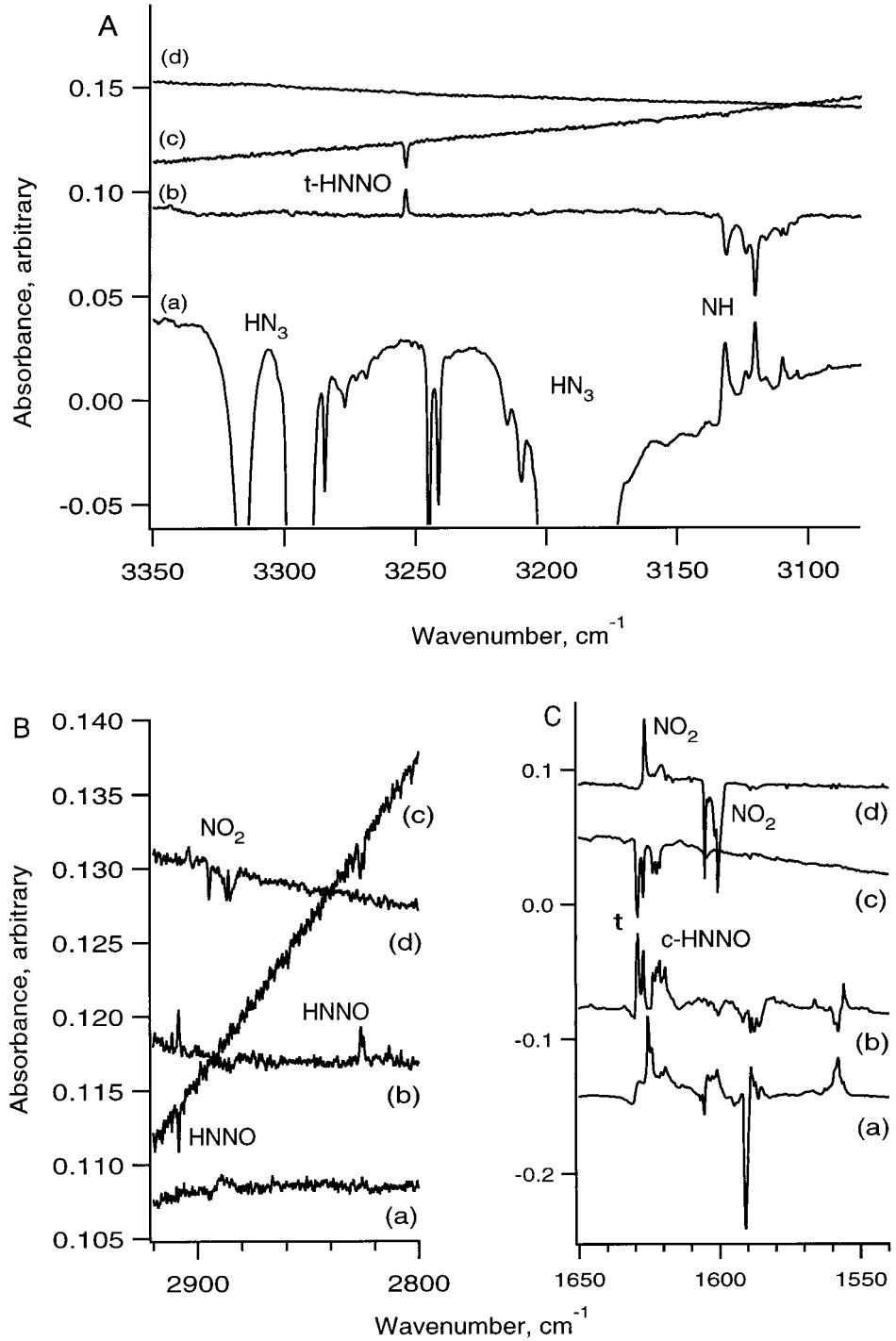

Figure 1. IR spectrum of HNNO. FTIR difference spectra (a−c) of a HN_3/NO/Xe 2.8:1:395 matrix (3.88 mmol) at 11 K. Plot A shows spectra in the region 3350−3080 cm^{-1}, plot B 2920−2800 cm^{-1}, plot C 1650−1540 cm^{-1}. Trace labels for all plots: (a) change, from deposition, upon 2.0 h photolysis at 254 nm; (b) change of sample a upon annealing to 44 K; (c) change of sample b upon 2.0 h photolysis at 550 nm. (d) FTIR difference spectrum of a NO/Xe 1:393 matrix (2.07 mmol) at 11 K. Change upon annealing sample to 40 K, after 2.0 h photolysis at 254 nm, for comparison with (b). t = *trans*-HNNO; c = *cis*-HNNO.

but indirect room light was not excluded. This distinguishing growth/loss behavior of type I and II bands is shown in the spectra of Figure 4 and depicted quantitatively in Figure 3.

The loss of bands I and II upon further photolysis is accompanied by slight growth of N_2O bands at 1280 and 2218 cm^{-1}. Since N_2O absorptions are present initially from impurities in the NO, and increase in intensity during photolysis, their relative increase is small, but the fact of an increase is reproducible. This behavior is included among the growth curves in Figure 3. Absorption bands of HONO grow in due to photolysis of HNOO.[30]

^{15}N-labeled nitric oxide was used in some experiments. In matrixes of HN_3/^{15}NO/Xe 2:1:400, infrared bands with the same growth and loss behavior are observed. After 254 nm photolysis, the split NH absorption near 3133 cm^{-1} is observed; it is depleted upon annealing as infrared bands with behavior like the I and II bands grow in. Isotope-shifted bands corresponding to product I are seen at 1594.7/1593.8, 1212.9/1211.6, 1285.2/1283.2, 3253.6, and 742.9 cm^{-1}. The isotope shifts (expressed as the isotope shift ratio, ν_{14}/ν_{15}) are included in Table 1. Shifted IR bands corresponding to product II are observed at 1590.7/1589.5/1588.6, 1163.8, 1260.7, 3156.9, and 706.7 cm^{-1}; the

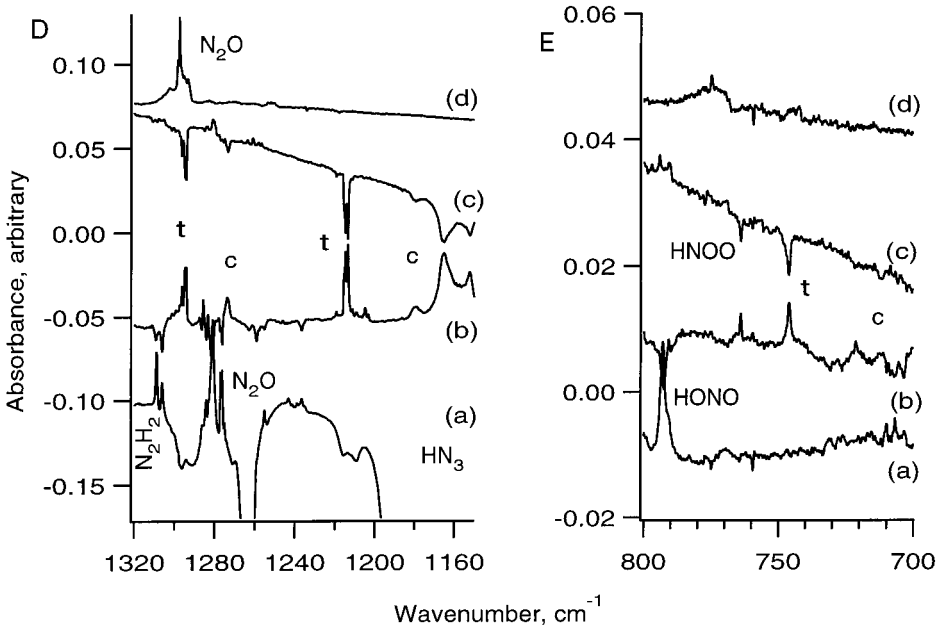

Figure 2. IR spectrum of HNNO. FTIR difference spectra for the samples in Figure 1. Plot D shows spectra in the region 1320−1150 cm^{-1}, plot E 800−700 cm^{-1}. Trace labels are the same as in Figure 1.

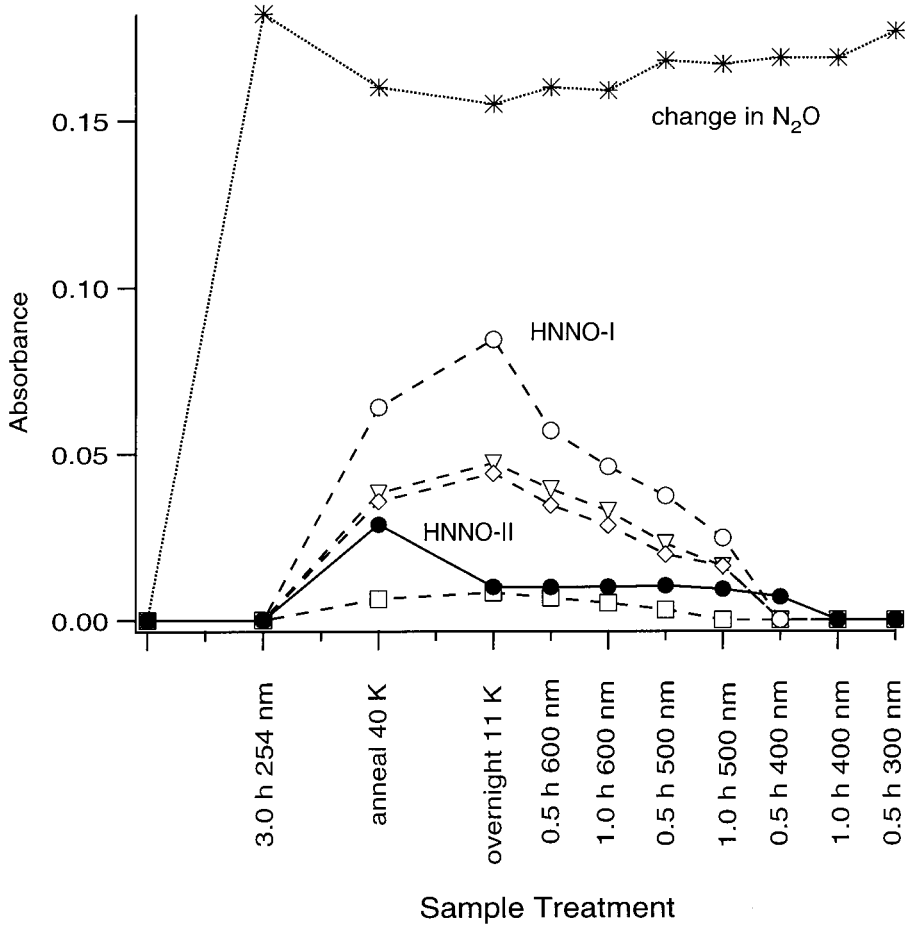

Figure 3. Growth and loss of HNNO as a function of sample treatment. Absorbance of selected bands measured as peak height for changes in a HN_3/NO/Xe 2.3:1:401 matrix (4.0 mmol) at 11 K upon photolysis and annealing sequence as described in text. Open symbols with dashed lines refer to *trans*-HNNO: circles = 1628 cm^{-1} absorption; triangles = 1213 cm^{-1} absorption; diamonds = 1294 cm^{-1} absorption; squares = 746 cm^{-1} absorption. Solid circles with a solid line refer to *cis*-HNNO, 1621 cm^{-1} absorption. Stars with dotted line refer to the change in the N_2O absorbance at 1280 cm^{-1}, expressed as the difference in absorbance from the sample initially deposited.

isotope shift ratios for these bands are included in Table 2. Bands at 2821.5/2814.1 and 2756.0/2747.6 cm^{-1} exhibit the behavior common to types I and II, growth upon annealing and loss upon long-wavelength photolysis, but were too weak to be identified definitively as type I or II. They are listed with the type I bands in Table 1. FTIR spectra for a ^{15}NO labeling experiment are shown in Figure 5, traces a−c and again display the "mirror-image" appearance that is characteristic of the bands I and II.

TABLE 1: Comparison of Experimental Frequencies, Intensities, and $^{14}N/^{15}N$ Isotope Ratios for Isomer I with Calculated Frequencies for *trans*- and *cis*-HNNO[a]

		experiment			CCI−CASSCF Walch[25]		MP2 6-31G Durant[15]		HF 6-31G Harrison[48]
mode	isotopomer	$\nu(14)$ $\nu(15)$	*A* rel.	14/15 ratio	$\nu(14)$ trans	$\nu(14)$ cis	$\nu(14)$ trans	$\nu(14)$ cis	$\nu(14)$
ν_1 NH str	$HN^{14}NO$	3254.0	18	1.0001	3311	3160	3713	3600	3568
	$HN^{15}NO$	3253.6	16						
ν_2 NN str	$HN^{14}NO$	1628.9	**100**	1.0208	1628	1630	1562	1640	1669
		1627.1	81	1.0209					
	$HN^{15}NO$	1594.7	**100**						
		1593.8	77						
ν_3 NO str	$HN^{14}NO$	1296.2	40	1.0086	1382	1373	1422	1449	1450
		1294.5	55	1.0088					
	$HN^{15}NO$	1285.2	46						
		1283.2	69						
ν_4 HNN bend	$HN^{14}NO$	1214.7	56	1.0015	1228	1201	1125	1167	1178
		1213.4	65	1.0015					
	$HN^{15}NO$	1212.9	56						
		1211.6	61						
ν_6 torsion	$HN^{14}NO$	746.5	10	1.0048	797	771	1005	941	925
	$HN^{15}NO$	742.9	13						
ν_5 NNO bend	$HN^{14}NO$		n.o.		549	589	322	353	448
	$HN^{15}NO$		n.o.						
$\nu_2 + \nu_3$ comb.	$HN^{14}NO$	2911.6	wk						
		2908.7	wk						
	$HN^{15}NO$	2821.5?							
		2756.0?							
$\nu_2 + \nu_4$ comb.	$HN^{14}NO$	2826.5							
		2825.1							

[a] The top row in the section for each mode refers to the normal $HN^{14}NO$ isotopomer. 14/15 ratio as described in the text. *A* rel. = relative absorbance as peak height, scaled such that *A* of the NN stretching mode for isomer I (strongest observed band) = 100. wk = weak; n.o. = not observed.

TABLE 2: Comparison of Experimental Frequencies, Intensities, and $^{14}N/^{15}N$ Isotope Ratios for Isomer II with Calculated Frequencies for *trans*- and *cis*-HNNO[a]

		experiment			CCI-CASSCF Walch[25]		MP2 6-31G Durant[15]		HF 6-31G Harrison[48]
mode	isotopomer	$\nu(14)$ $\nu(15)$	*A* rel.	14/15 ratio	$\nu(14)$ trans	$\nu(14)$ cis	$\nu(14)$ trans	$\nu(14)$ cis	$\nu(14)$
ν_1 NH str	$HN^{14}NO$	3158	v. wk	1.0003	3311	3160	3713	3600	3568
	$HN^{15}NO$	3156.9							
ν_2 NN str	$HN^{14}NO$	1623.7	71	1.0207	1628	1630	1562	1640	1669
		1622.3	61	1.0206					
		1621.4	76	1.0206					
	$HN^{15}NO$	1590.7	100						
		1589.5	54						
		1588.6	55						
ν_3 NO str	$HN^{14}NO$	1273.4	23	1.0101	1382	1373	1422	1449	1450
	$HN^{15}NO$	1260.7	20						
ν_4 HNN bend	$HN^{14}NO$	1166.9	24	1.0027	1228	1201	1125	1167	1178
	$HN^{15}NO$	1163.8	44						
ν_6 torsion	$HN^{14}NO$	712.1	5	1.0076	797	771	1005	941	925
	$HN^{15}NO$	706.7	5						
ν_5 NNO bend	$HN^{14}NO$		n.o.		549	589	322	353	448
	$HN^{15}NO$								

[a] The top row in the section for each mode refers to the normal $HN^{14}NO$ isotopomer. 14/15 ratio as described in text. *A* rel. = relative absorbance as peak height, scaled such that *A* of NN stretching mode (strongest observed band for Isomer II) = 100. v. wk = very weak; n.o. = not observed.

The frequencies and assignments of other bands observed in these experiments are included in Table S1 of the Supporting Information.

^{15}N isotope studies were also performed on matrices containing only NO and Xe to assist in identifying the bands of NO dimers. Spectra from a mixed-isotope study using both ^{14}NO and ^{15}NO clearly identify the dimers by the spectral splitting into three bands due to singly and doubly labeled symmetrical dimers. Isolated ^{15}NO is seen at 1833.8 cm^{-1}, and the $(^{15}NO)_2$ bands shift to near 1822 cm^{-1} (1840 cm^{-1} in the mixed dimer) and 1715 cm^{-1} (1727 cm^{-1} in the mixed dimer). Isotope shifts for the NO_2 and N_2O impurities help identify these bands as well. The spectrum of an ^{15}NO/Xe 1:400 sample treated in the same manner as the $HN_3/^{15}NO$/Xe samples is shown in trace d of Figure 5. The sample has been annealed following 254 nm photolysis, conditions which produce species I and II in xenon matrices containing HN_3 along with NO.

Discussion

Spectroscopy. *Spectroscopy and Reactions of Nitrogen Oxides.* The purpose of this section to identify the matrix

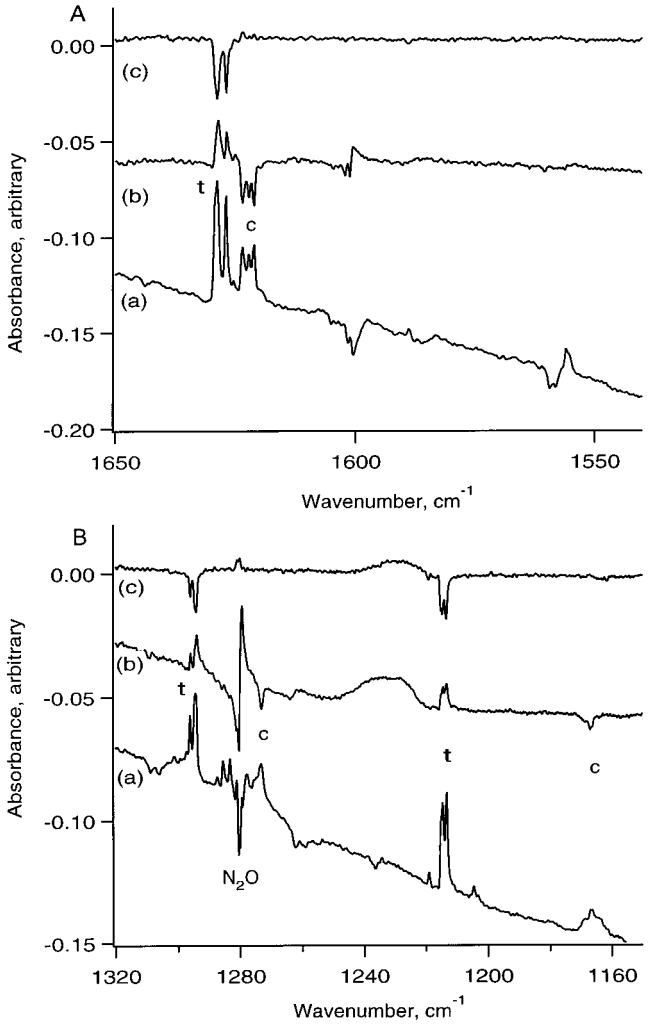

Figure 4. Cis−trans isomerization of HNNO. FTIR difference spectra of a HN_3/NO/Xe 2.3:1:401 matrix (4.0 mmol) at 11 K. Plot A shows spectra in the region 1650−1540 cm^{-1}, plot B 1320−1150 cm^{-1}. Trace labels for both plots: (a) change upon annealing to 40 K, after 3.0 h photolysis at 254 nm; (b) change of sample a upon holding overnight at 11 K; (c) change of sample b upon 1.0 h photolysis at 600 nm.

chemistry of the nitrogen oxides to the extent needed to distinguish it from reactions involving the NH reactant, since both NH-dependent and NH-independent processes occur under our experimental conditions. One prominent process for which evidence is visible in the initial sample is NO dimerization. The spectroscopy and reactions of NO dimers have been studied in detail in other matrices,[32,33] and these findings can be used to assign and interpret the observations in Xe. The vibrational bands for the NO dimers are readily identified by their isotope shifts in the experiments using ^{15}NO or a mixture of ^{14}NO and ^{15}NO. The isotope shift ratio of 1.018 for both bands of the doubly substituted NO dimer near 1854 and 1745 cm^{-1} is identical to the ratio observed for NO monomer at 1866 cm^{-1}. The isotope shift ratio for the mixed $^{14}NO-^{15}NO$ dimer is 1.0076 for the ν_1 symmetric stretch and 1.0102 for the ν_5 antisymmetric stretch; the product of these shifts is 1.0179. Only the more stable *cis*-$(NO)_2$ species is identified; although several other bands occur in the NO stretching region and exhibit ^{15}NO shifts near 1.018, suggesting they contain an NO chromophore, none had an isotope substitution pattern that identified them as dimers. They may be due to complexes of NO with other species, perhaps an NO−Xe complex or NO−HN_3. Other nitrogen oxides, for example N_2O_3, have bands in the same region[45] but would be expected to show isotope shifts involving two nitrogen atoms. The isotope shift ratios for NO_2 and N_2O impurities are in good agreement with published isotope shift data for ^{15}N-labeled species.[34,35]

Upon 254 nm photolysis, the dimer bands decrease in intensity and the monomer band increases in intensity. Annealing regenerates the dimers at the expense of the monomer. The changes in N_2O and NO_2 are complex, depending on the detailed deposition conditions, temperature history, and concentration of the sample, but in general the amounts of both species increase upon 254 nm photolysis and changes occur as well upon annealing, particularly site interconversion. The major processes observed here are consistent with the observations in Ne and N_2 matrix.[33] $(NO)_2$ photodissociates to NO under UV irradiation and the dimers reform upon annealing. Photoreaction of dimers to form both NO_2 and N_2O in the matrix has also been reported, although the specific processes that lead to each product are matrix- and temperature-dependent.[33] The use of xenon matrix may further complicate both the spectroscopy and the dynamics of dimer association, dissociation, and reaction, as the binding energy of NO with Xe may be comparable or in excess of that of the NO dimer, about 2.0 kJ mol^{-1}.[46] Xenon complexes may form with the other nitrogen oxides, especially NO_2, and may explain the multiple trapping sites that are evident in the spectrum and undergo interconversion during photolysis and/or annealing.

While the changes observed for the nitrogen oxides are complex, they can be clearly distinguished from the behavior of the absorption bands described above and designated I and II. In contrast with the nitrogen oxide bands, the I and II bands (1) appear only when HN_3 and NO are both present in the matrix, (2) are visible neither upon initial deposition nor after either 254 nm photolysis or annealing of a matrix after deposition, (3) appear only after a matrix is treated by 254 nm photolysis then annealing, in that order, and (4) can then be destroyed by irradiation at wavelengths of 500 to 600 nm.

Assignment of Bands of Product I. The evidence above indicates that NH and NO participate in the reaction and that a stable species is formed that can then be destroyed by a low-energy photochemical process. The reaction expected to occur between ground-state NH and NO is the activationless addition to form HNNO. The conditions of appearance and disappearance of I are consistent with formation of a stable radical such as HNNO. As will be shown, the infrared spectrum of product I is consistent with bent planar HNNO in a ground $^2A'$ state, the structure of which is best represented, in a valence-bond model, by the structure below. To support this conclusion, the assignments of individual vibrational modes are now discussed.

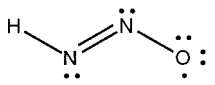

The strong bands at 1628 and 1294 cm^{-1} are assigned to the ν_2 and ν_3 NN and NO stretches. Both bands are split into doublets, with a splitting of about 2 cm^{-1} as is typical of site splittings in xenon matrix. These bands lie strikingly close to the corresponding antisymmetric and symmetric stretches of the isoelectronic molecule NO_2, at 1618 and 1318 cm^{-1} (in the gas phase).[35] The ^{15}NO isotope shift ratio of 1.0208 for the 1628 cm^{-1} band and 1.0088 for the 1294 cm^{-1} band are also very close to the isotope shift ratios of 1.0241 and 1.0092 for ^{15}N-labeled NO_2.[35] The NN bond can be considered a double bond by comparison with the similar frequencies of the N═N

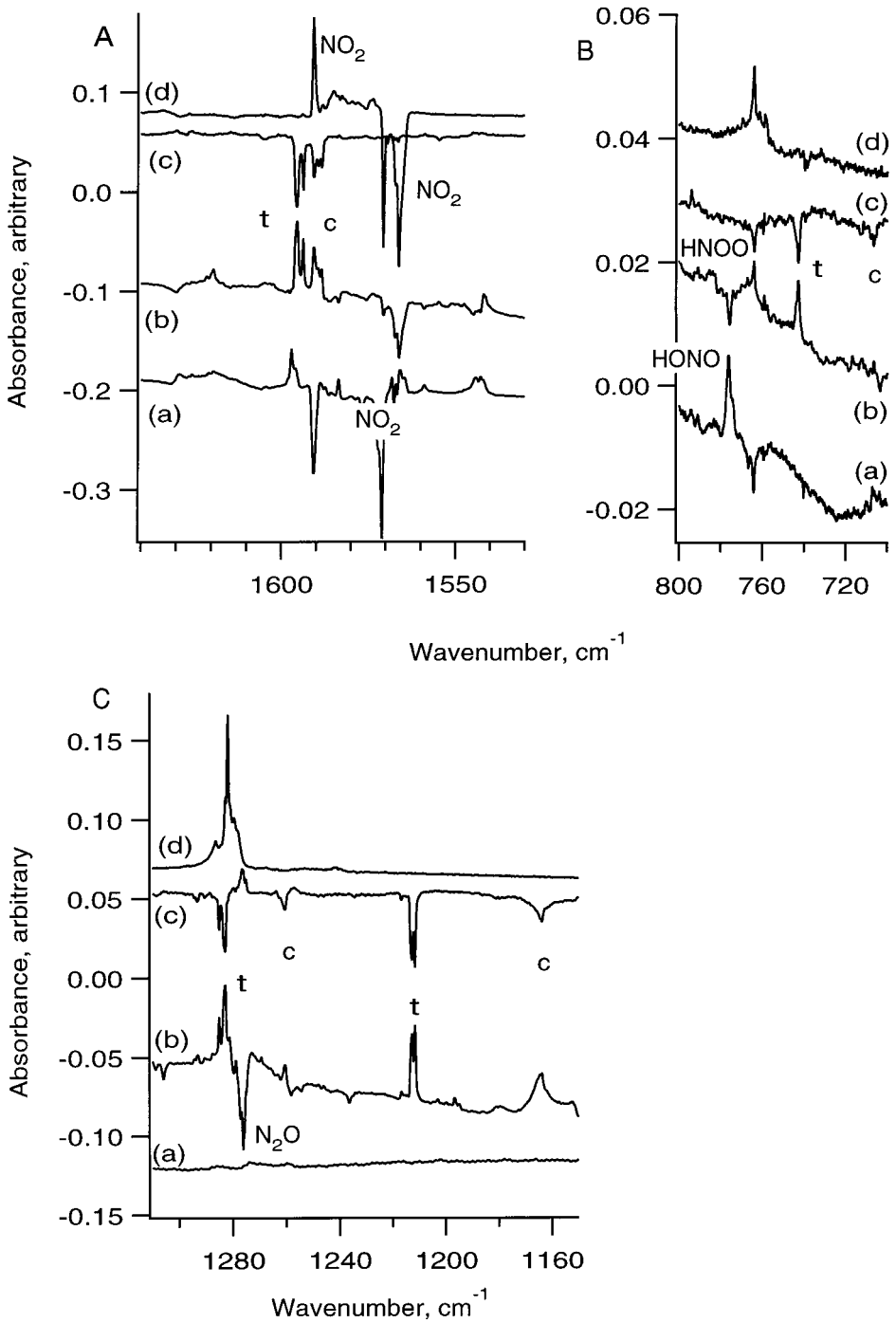

Figure 5. Isotope labeling of HNNO. FTIR difference spectra (a−c) of an HN_3/^{15}NO/Xe 2:2:400 matrix (3.72 mmol) at 11 K. Plot A shows spectra in the region 1640−1530 cm^{-1}; plot B 800−700 cm^{-1}; plot C 1310−1160 cm^{-1}. Trace labels for all plots: (a) change from deposition upon 2.0 h photolysis at 254 nm; (b) change in sample a upon annealing to 42 K; (c) change in sample b upon photolysis to total photodepletion of HNNO. (d) FTIR difference spectrum of a ^{15}NO/Xe 1:399 matrix (2.11 mmol) at 11 K. Change upon annealing sample to 40 K after 2.25 h photolysis at 254 nm, for comparison with (b).

stretching vibrations of NNH_2 at 1574 cm^{-1} (Ar) and HNNH at 1529 cm^{-1} (N_2).[31] It is quite distinct from the N≡N stretch of N_2O (2224 cm^{-1} gas)[34] and the N≡N stretch (2133 cm^{-1}) and N−N stretch (1145 cm^{-1}) of HN_3 (Xe, this work). The NO bond has partial double bond character if the stretching frequency is judged in comparison with the N═O bond of HNO at 1565 cm^{-1} (gas),[45] the N═O stretch of HONO (cis 1626, trans 1680 cm^{-1} in Xe), the N═O stretch of HOONO at 1704 cm^{-1} (Ar),[47] and the N−O stretch of HONO (cis 842, trans 791 cm^{-1} in Xe). The NN bond is expected to have more double-bond character than the NO bond and thus the higher frequency band is labeled as the NN stretch, but clearly the two stretching modes are strongly coupled as in NO_2.

The vibrational frequencies for HNNO have been calculated by several workers.[15,25,48] Because of the treatment of electron correlation, the CCI/CASSCF calculations by Walch[25] are expected to predict the vibrational frequencies for this radical better than the MP2 calculations of Durant[15] and the Hartree−Fock method of Harrison and Maclagan.[48] Thus, our discussion focuses on the calculations by Walch, but the other published values are included in Tables 1 and 2 as well. As seen in Table 1, the calculated NO and NN stretching frequencies for either

trans-HNNO or *cis*-HNNO are in quite good agreement with the observations.

It follows from the stretching band assignments that the absorption at 2908 cm^{-1} is due to the combination band $\nu_2 + \nu_3$, close to the sum of the fundamental frequencies at 2922 cm^{-1}, and also very close to the analogous NO_2 combination band $\nu_1 + \nu_3$ at 2907 cm^{-1}.[49] In isoelectronic molecules such as NO_2 and the CO_2^- ion,[50] this combination band is stronger than the ν_1 and ν_2 fundamentals. Thus, for HNNO it is not surprising that this combination band is sufficiently intense to be observed. The band at 2826 cm^{-1} is assigned to the $\nu_2 + \nu_4$ combination band, near the frequency sum of 2842 cm^{-1}. Absorptions at 2821.5/2814.1 and 2856.0/2747.6 cm^{-1} are observed in the ^{15}NO-labeled experiment. If these are assigned to the two combination bands, the observed isotope shift ratios, 1.032 and 1.026, respectively, are rather large compared to the shift ratios expected from the sums of the shifted frequencies. However, it may be that these bands do not correspond to the same set of bands, I or II, if isotope labeling alters the relative intensities of the combination bands.

The 3254.0 cm^{-1} absorption is assigned to the ν_1 NH stretch. The frequency is comparable to HN_3 at 3298 cm^{-1} (Xe) and free NH at 3131 cm^{-1} (Xe). Its lack of an isotope shift shows that this mode is largely uncoupled to the other vibrations. The observed value lies between the computed values for *cis*- and *trans*-HNNO.[25]

The band at 1213.4 cm^{-1} is assigned to the ν_4 HNN bend. Its frequency is similar to the HNN bend in HN_3 (1263 cm^{-1} in Xe, this work), the H_2N rocking motion of H_2NN (1288 cm^{-1}, Ar),[31] and the NH bend of HN═NH (1313 cm^{-1}, Ar).[31] The small ^{15}N isotope shift (1.0015) reflects the fact that most of the atomic motion is in the light H atom. The experimental frequency is in good agreement with the calculated frequency for either HNNO isomer. The remaining band at 746.5 cm^{-1} is assigned to the ν_6 out-of-plane mode, with a modest isotope shift (1.0048). It is comparable to the torsional mode of HNOO at 764 cm^{-1} (Xe),[30] HN_3 at 607 cm^{-1} (gas),[35] and HONO at 638 cm^{-1} (cis, Ar) and 549 cm^{-1} (trans, Ar).[40] Again, the experimental frequency for this mode is consistent with the calculated frequency for either *cis*- or *trans*-HNNO. The NNO bend is not observed. It is calculated by Walch to fall at 549 cm^{-1} (trans) and 589 cm^{-1} (cis).

On the basis of this spectroscopic evidence, we conclude that the absorptions labeled I belong to an isomer of the radical intermediate HNNO, formed from the reaction of ground-state NH with NO.

Assignment of Bands of Product II. The bands in the set designated II have the same "mirror-image" behavior as the bands of I; they appear upon annealing a matrix containing NO and trapped NH and disappear upon irradiation at wavelengths as long as 600 nm. It is clear that they, like I, belong to a stable transient that is readily destroyed by a low-energy photochemical process. The bands also lie close in wavenumber to the first set of bands, identified as HNNO. Bands at 1623 and 1273 cm^{-1} lie within 5 and 23 cm^{-1}, respectively, of the features of I assigned to the NN and NO stretches. A band at 3158 cm^{-1} is less than 100 cm^{-1} (3%) from the band of I assigned to the NH stretch of HNNO. Bands also lie close to each group I absorption assigned to a bending vibration of HNNO. The feature at 1167 cm^{-1} corresponds to the 1214 cm^{-1} band assigned to the HNN bend, while the absorption at 712 cm^{-1} lies near the I band assigned to the torsion at 746 cm^{-1}. Since HNNO is expected to be a planar molecule with cis and trans isomers, the similarity of the infrared spectra of I and II suggests that II is, like I, an isomer of HNNO. The isotope shift ratios of II are similar to those of I but sufficiently different that it is clear they are not the same molecule. Thus, the spectroscopic arguments presented above for the identification of I with HNNO apply equally to the bands of II. The frequency differences observed between corresponding bands of I and II (5−50 cm^{-1} for the fingerprint region, 100 cm^{-1} for the high-frequency bands) are consistent with the splittings observed for geometric isomers of similar planar, tetraatomic molecules such as HONO.[31,40] The splittings are larger than expected for matrix site splittings.

The type II bands vary in intensity relative to the type I bands and were not observed at all in some experiments. Although frustrating attempts to gather more information about this species, this observation is consistent with the identification of II as a second, less stable isomer of HNNO. If the I and II bands represent two isomers with a small energy difference, both formed in a reaction with a larger exothermicity than the barrier between them, their relative population will be sensitive to the temperature history of each sample during the annealing process. Formation of the two isomers in a matrix may also be influenced by the microscopic site distribution of the NH and NO precursors, itself a function of the details of matrix preparation and photolysis. These microscopic variables undoubtedly vary among samples whose gross properties (concentration, maximum annealing temperature, annealing time) are nevertheless similar. Finally, we observed interesting behavior upon 700 nm photolysis or prolonged storage at 11 K of a sample containing both I and II bands (Figure 4, trace a). As seen in trace b of Figure 4, the bands of II disappear, while the I bands increase in intensity. The simplest explanation for this behavior is a conversion of II to I, a process evidently requiring less energy than destruction of both I and II (Figure 4, trace c; Figures 1 and 3). On the basis of the combined spectral and chemical evidence, we conclude that the bands of II are those of a second HNNO isomer.

Which Isomer is Which? The discussion above identifies both I and II as HNNO isomers but has not yet addressed which isomer is which. The calculated frequencies do not appear to settle the matter, since the observed infrared bands agree reasonably with the calculated vibrational spectrum of either *cis*- or *trans*-HNNO. However, the calculations do help address this issue if we consider the relative frequencies of *cis*- and *trans*-HNNO rather than the absolute magnitudes of the frequencies. If we consider the frequency differences observed for the five bands, $\Delta\nu_{exp} = (\nu_I - \nu_{II})$, expressed as a percentage of ν_I, we find that $\Delta\nu_{exp}$ is always positive; that is, the I frequencies are always higher. The differences show the following pattern: the ν_2 bands are almost the same ($\Delta\nu_{exp}$ = 5 cm^{-1} or 0.3%), a modest difference of about +1.6% is seen in ν_3, and larger differences of +3−5% are observed for ν_1, ν_4, and ν_6. When these are compared to the differences in the calculated frequencies for *cis*- and *trans*-HNNO,[25] $\Delta\nu_{calc} = (\nu_{trans} - \nu_{cis})$, it is seen that the trans frequencies are always the higher ones, except for ν_2 where the difference is essentially zero ($\Delta\nu_{calc} = -2$ cm^{-1} or −0.1%). Moreover, the differences can be grouped in the same way, a near-zero difference in ν_2, a modest difference in ν_3 of 0.7%, and larger differences of +2−5% in ν_1, ν_4, and ν_6. Thus, the pattern of cis−trans splitting in the calculated frequencies is quite similar to the pattern of I−II splitting in the experimental frequencies if I is identified as *trans*-HNNO and II as *cis*-HNNO.

Thermodynamic evidence is consistent with this assignment of isomers. The trans isomer is calculated to be more stable by about 24 kJ mol^{-1}.[15,25] Our observations support the interpreta-

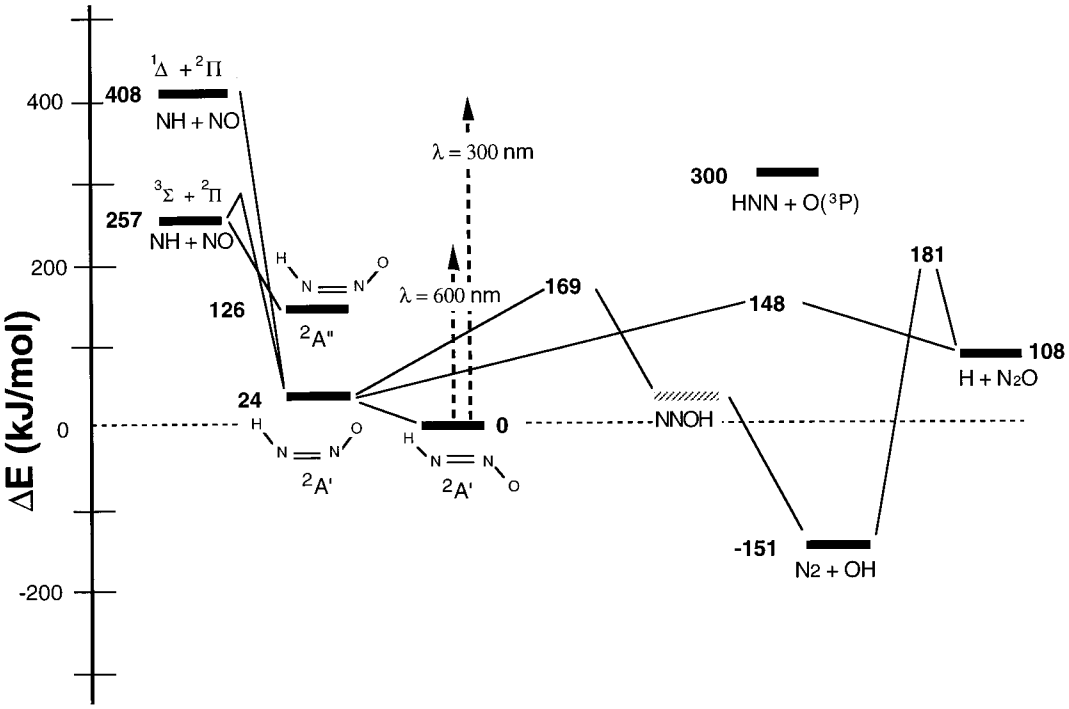

Figure 6. Energy level diagram for the HNNO system. Energies taken from "best estimate" energies from Bradley et al., ref 27, and, where "best estimate" values were not available, from Walch, ref 25. The HNN + O (^{3}P) energy is from Bozzelli & Dean, ref 23.

tion that I is the more stable isomer; it is initially formed in greater quantity (assuming comparable IR absorptivities), and II is preferentially converted to I, rather than the reverse reaction, when activation energy is available. On the basis of the spectroscopic and thermochemical arguments, we assign the set of bands I to *trans*-HNNO and the II bands to *cis*-HNNO. High-level calculations of the vibrational frequencies of the isotope-substituted species would be helpful in confirming this assignment.

Reaction Chemistry of HNNO. From the experimental evidence, some information about the thermochemistry of the novel species HNNO can be deduced and compared with theoretical predictions. The energy level diagram calculated for this system is shown in Figure 6 and should be referred to during the following discussion. We have used the "best estimate" energies from Bradley et al.,[27] which draw on published calculations by Walch[25] and Durant.[15] The latter calculations use different methods, both of which are expected to give high-quality energies for the stationary points, and the agreement between these two reports is generally very good, as discussed by Durant.

Formation and Trapping of HNNO. According to Walch,[25] the reaction of NH ($X\ ^3\Sigma^-$) with NO is activationless on the $^2A''$ surface because the singly occupied NO 2π orbital lies in the same plane as the HN−NO supermolecule. The small barrier on the ground $^2A'$ surface arises because the singly occupied orbital is perpendicular to the plane, thus NH is adding to an NO π bond. Thus, reaction 1 proceeds initially on the $^2A''$ surface. Crossing to the lower-energy $^2A'$ surface is made possible by out-of-plane motions that break the C_s symmetry.

The exothermicity of reaction 1, nearly 260 kJ mol^{-1}, is more than sufficient to overcome the barriers to the energetically accessible final products, H + N_2O or OH + N_2. In the gas phase, fragmentation of the HNNO is rapid and only final products are observed.[8,14,15] In contrast, the matrix experiments use conditions that make it possible to trap HNNO. Both reactants are internally and translationally precooled to 11 K, then collided very gently at temperatures no higher than 45 K. The surrounding matrix cage both sustains the collision complex long enough for reaction to occur and effectively removes energy so that the complex does not dissociate from the reaction exothermicity.

Theory predicts that HNNO should also be formed in the reaction of NH (a $^1\Delta$) with NO, but HNNO was not observed in the argon matrix studies by Yokoyama et al.[12] Other than the use of Ar matrix, their experiments were quite similar to the present work, using 254 nm photolysis of HN_3 as the NH source and comparable HN_3/NO/rare gas ratios. It is likely that HNNO was not formed in those experiments because the reaction exothermicity for formation of HNNO from NH (a $^1\Delta$) + NO, over 400 kJ mol^{-1}, made it impossible for the HNNO intermediate to be stabilized.

Annealing of the matrix to 40−44 K maximizes the yield of HNNO. Higher temperatures increase the prevalence of side reactions such as dimerization of NO and formation of NO_2. Infrared absorptions of the HNNO complex are detected at lower temperatures, 20−30 K, during the annealing process, suggesting that the small barrier to HNNO formation is associated with diffusion and/or reorientation of the reactants in the matrix and not with a barrier intrinsic to the reaction. Atoms similar in size to NH, such as fluorine and oxygen, are quite mobile in matrices,[51,52] and O (^{3}P) atoms, isoelectronic with NH, are known to escape the matrix cage with a low activation energy.[53,54] Similar annealing temperatures are optimal in forming HNOO from NH (X) + O_2 in Xe, a reaction also expected to be activationless.[30]

Annealing can mobilize other atoms and small molecules besides NH, so the possibility of other reactions must be considered. Reaction of H + N_2O is one alternate route to formation of HNNO, since N_2O was an impurity in most samples. Formation of H atoms is thermochemically feasible from HN_3 photolysis, though the absence of N_3 absorptions after photolysis indicates that this is at best a minor channel in the matrix. Further evidence for H atoms in these samples might

be sought from the formation of HXeH, which is known to occur readily when H atoms are mobilized in Xe matrix.[55,56] The strongest absorption of this species, at 1166 cm^{-1}, lies close to an absorption we have assigned to *cis*-HNNO. However, the disappearance of this feature upon long-wavelength ($\lambda \leq 600$ nm) photolysis is not consistent with the resistance to photobleaching by a broadband visible source that has been described,[55] and HXeH should not exhibit the isotope shift we observe when ^{15}NO is used. Thus, although we cannot rule out formation of H atoms in these samples, we have no good evidence for such a process. More importantly, as Figure 6 shows, there is a barrier to formation of HNNO from $H + N_2O$. Thus, although the annealing temperatures used are sufficient to mobilize any H atoms that may be trapped in the matrix, they are not sufficient to overcome this barrier. Together these factors argue against $H + N_2O$ as a source of HNNO in these experiments.

Photolysis of NO_2 or N_2O could provide another reactive radical, O (^3P), that would be invisible in the matrix. Reaction of O with NNH might also yield HNNO in an exothermic reaction. However, there is no straightforward route to produce the other reactant, NNH, via 254 nm HN_3 photolysis. Moreover, NNH is believed to be unstable relative to $N_2 + H$.[23,24] The simplest explanation that is consistent with all our observations, including direct observation of the loss of NH upon annealing, is that NH is mobilized upon annealing and is the major reactive species.

The use of xenon matrix in these studies is not gratuitous. Its most important role appears to be in preparing the NH (X) reactant. HN_3 photodissociates to form electronically excited NH (a $^1\Delta$). Electronic quenching of NH (a) is very slow, on the order of a second in solid argon,[39] and numerous studies show that NH (a $^1\Delta$) is very reactive in a matrix. Thus, in the argon matrices commonly used in matrix isolation, chemical reaction of NH (a) will take place faster than intersystem crossing. Very little NH will escape reaction to become trapped in the matrix in the ground electronic state and thus become available for reaction upon annealing. In xenon matrix, however, the external heavy-atom effect enhances the rate of intersystem crossing from the initially formed singlet to the ground triplet surface of NH, and indeed the NH (a) lifetime in solid Xe shows evidence for a strong external heavy-atom effect.[39] Evidently intersystem crossing becomes competitive with bimolecular reaction, so that significant amounts of NH (X) are trapped. This interpretation is further supported by studies of HN_3 photolysis in Ar and Xe, in which the relative IR intensity of NH product is indeed higher in Xe than in Ar.[57] Because NH is a weak IR absorber,[58] the amount of trapped NH observed in Xe represents a substantial fraction of the photolyzed HN_3.

Substantial matrix effects on product yields in bimolecular reactions, including those of NH, have been observed previously.[30,59−62] In our previous studies of the reaction of NH with O_2, the Ar matrix yielded mostly HONO and only very small amounts of HNOO, while in Xe the relative yields of these species were completely reversed.[30] HONO is produced upon initial 254 nm photolysis by reaction of NH (a $^1\Delta$) with O_2, while HNOO is produced by reaction of NH (X $^3\Sigma^-$) with O_2 upon annealing. Thus, in that example, the relative importance of electronic quenching vs chemical reaction of the initially formed NH (a) radicals was reversed upon changing the matrix material from Ar to Xe. In the reaction of NH with dimethylacetylene, the major product in Xe was not observed at all in Ar, reflecting different chemical reaction channels available from the singlet vs triplet reaction surfaces.[59] In the present work, no HNNO is observed after the initial photolysis. Apparently direct reaction of NH (a) with NO is slower than quenching in Xe. Gas-phase workers have taken advantage of the same phenomenon, adding small amounts of Xe to a reaction mixture to convert NH (a) to NH (X) in the presence of NO.[8,14] Formation of small amounts of HONO and NH_2OH, produced by the well-known reactions of NH (a $^1\Delta$) with matrix impurities O_2 and H_2O,[30,63−66] shows that chemical reactions of NH (a) more rapid than that with NO can still compete with quenching in Xe.

While the effect of Xe on NH electronic states most likely explains the ability to produce HNNO in Xe matrix, the solid-state structure of xenon may also play a role. Imidogen radicals may be more mobile in Xe than Ar due to the larger cage size and the heterogeneity (probably substantial) of the polycrystalline matrix. Xenon matrix can be warmed to a higher temperature than an argon matrix, so it is possible to anneal and induce reaction without affecting the sample's optical clarity too much. Complexation with xenon may help stabilize the intermediate once it is formed. Xenon-doping experiments in other matrix materials might shed some light on these issues.

In sum, to maximize our chances of detecting HNNO, the experiments reported here were performed in solid xenon matrix, where NH ($^3\Sigma^-$) could be selectively produced, where the only barrier to reaction with NO should be due to diffusion of the reactants in the solid, and where the intermediate would be rapidly cooled, preventing fragmentation.

Reaction of HNNO to Form Products. At the photolysis energies at which photodepletion of HNNO is first observed, the major product of HNNO destruction in these experiments appears to be N_2O, with an H atom presumably trapped nearby in the matrix cage. $N_2O + H$ is also the major channel in the gas phase, though $OH + N_2$ is also detected. Both channels are energetically accessible at $\lambda = 600$ nm (200 kJ mol^{-1}). The OH absorption at 3530 cm^{-1} in Xe[67] was not observed in these experiments; however, detection sensitivity in this region was low in many samples after annealing, due to increased matrix scattering in the high-frequency region. It is also possible that OH production is particularly inhibited in the matrix. From geometric considerations, the *cis*-HNNO isomer is the necessary precursor for the 1,3-hydrogen transfer to form $OH + N_2$. In the gas phase, reaction of an equilibrium mixture of cis and trans isomers would be expected, since the barrier to product formation is higher than the barrier to isomerization. But at the low temperatures of the matrix, the equilibrium may strongly favor the lower energy isomer even if the energy difference is very small. Thus, it is possible that all the starting material is in the trans form at the time of reaction and the $OH + N_2$ channel is not available. Another difference between these experiments and previous work is that the energy needed to overcome the barrier from HNNO to final products is delivered photochemically rather than as thermal energy. The reaction may be governed fully or partially by the contours of the potential energy surface of the absorbing excited state of HNNO, which has not been characterized, rather than by the ground-state surfaces discussed here.

Barriers to reaction can be estimated from the photolysis energy required to cause reaction. At 700 nm, cis−trans isomerization occurred but there appeared to be no net loss of HNNO nor formation of other products (without knowing IR absorptivities we cannot confirm mass conservation in the HNNO isomerization, but the increase in trans absorbance is roughly equal to the decrease in cis absorbance). This photon energy, equivalent to 171 kJ mol^{-1}, exceeds the barrier to

isomerization computed as 105 kJ mol^{-1} by Durant[15] and 85 kJ mol^{-1} by Fueno et al.[11] The possibility of isomerization occurring at even lower photon energies is intriguing but was not investigated fully. We do not assume that isomerization seen upon storage for several hours at 11 K indicates a very low barrier to isomerization, but rather that energy was available from some source not accounted for. Infrared radiation from the spectrometer source beam can be excluded as a cause, so our best explanation of this phenomenon is that room light induced isomerization; it deserves further investigation.

The threshold for photodepletion of HNNO is observed at $\lambda = 600$ nm, or 200 kJ mol^{-1}. This surpasses the computed barrier for the lowest barrier route (that to H + NO_2), 149 kJ mol^{-1}. However, net destruction of HNNO did not appear to predominate at 700 nm (171 kJ mol^{-1}), even though this energy too exceeds the computed barrier. We suggest that an absorbing excited electronic state of HNNO lies at a vertical transition energy between 171 and 200 kJ mol^{-1}. After absorption, internal conversion to the ground-state surface leads to formation of products.

At the higher photolysis energies ($\lambda \geq 400$ nm or 299 kJ mol^{-1}), a more rapid disappearance of HNNO relative to the lower photon energies is observed (see Figure 4). It is interesting to consider the possibility that a new product channel is opened at these energies. Some redissociation to NH + NO may occur, though we do not observe recovery of the NH absorption band. The O + NNH pathway also becomes energetically accessible from HNNO.[8,23] Dissociation of HNNO into O + NNH is analogous to the well-known NO_2 dissociation into O + NO, which has a significant quantum yield at energies above about 285 kJ mol^{-1} ($\lambda \leq 420$ nm).[68] Guided by published ab initio vibrational frequencies for NNH,[69] we looked for evidence of a new product appearing after 300 nm photolysis that was not formed during the longer wavelength photolysis. We see no evidence for NNH formation in these studies. However, NNH may rapidly dissociate to N_2 + H, species undetectable in these experiments.[23,24]

Conclusions

The reaction of cold NH ($X\ ^3\Sigma^-$) with NO in solid xenon yields the novel intermediate HNNO. The use of xenon as the matrix material facilitates preparation of the NH ($X\ ^3\Sigma^-$) reactant from photolytically generated NH ($a\ ^1\Delta$). Annealing of the matrix containing NH (X) and NO permits the reaction to take place with essentially no activation energy, then the solid matrix rapidly stabilizes the hot intermediate so it can be trapped for spectroscopic study. Infrared frequencies, isotope shifts from the reaction with ^{15}NO, and computed frequencies support the assignment of cis and trans isomers, with the major product identified as *trans*-HNNO. The compound is thermally stable at 11 K but photochemically reactive; HNNO undergoes photochemical cis−trans isomerization at $\lambda = 700$ nm and photodissociates to N_2O + H at $\lambda \leq 600$ nm. The observed activation energies for these processes are consistent with computed energy barriers previously published.

These findings should contribute to the understanding of the NH + NO reaction in several ways. First, the long-postulated existence of the HNNO intermediate has been confirmed. Experimental evidence for formation of this intermediate in the H + N_2O and O + NNH reactions can now be sought. The observation of the vibrational frequencies of both *cis*- and *trans*-HNNO should make it possible for theorists to refine the potential energy surface in the region of the HNNO intermediate and therefore improve rate calculations and modeling of combustion dynamics.

Finally, we have demonstrated the use of a solid environment to selectively influence the dynamics of a chemical reaction and steer its product distribution toward a desired or unusual product. As exhibited in this study, such a strategy may be particularly useful in the study of radical−radical reactions and thus may facilitate the design of systems to store free radicals in solids for use as high-energy and high-density propellants.

Acknowledgment. S.L.L. acknowledges the many contributions of an outstanding team of undergraduate co-workers. She thanks Tom Massura, Forrest Duddles, and Dr. Don Knoechel for technical help and Dr. Rich Dissly for comments on the manuscript. She thanks Dr. Marilyn Jacox for valuable conversations about this work and for support, advice, and stimulating discussion of a wide variety of topics. A.E.D. and K.M. acknowledge Kalamazoo College for support by student−faculty research funds. The William and Flora Hewlett Fund of the Research Corporation supported this work. Equipment used in this study was funded by grants from the Petroleum Research Fund of the American Chemical Society and the National Science Foundation.

Supporting Information Available: A table summarizing the infrared frequencies, intensities, intensity changes, and band assignments for these experiments. This material is available free of charge via the Internet at http://pubs.acs.org.

References and Notes

(1) Dean, A. M.; Chou, M.-S.; Stern, D. In *The Chemistry of Combustion Processes*; Sloane, T. M., Ed.; ACS Symposium Series 249; American Chemical Society: Washington, DC, 1984; Chapter 5.
(2) Blint, R. J.; Dasch, C. J. In *The Chemistry of Combustion Processes*; Sloane, T. M., Ed.; ACS Symposium Series 249; American Chemical Society: Washington, DC, 1984; Chapter 6.
(3) Perry, R. A.; Siebers, D. L. *Nature* **1986**, *324*, 657.
(4) Cox, J. W.; Nelson, H. H.; McDonald, J. R. *Chem. Phys.* **1985**, *96*, 175.
(5) Harrison, J. A.; Whyte, A. R.; Phillips, L. F. *Chem. Phys. Lett.* **1986**, *129*, 346.
(6) Hack, W.; Wilms, A. *J. Phys. Chem.* **1989**, *93*, 3540.
(7) Hack, W.; Rathmann, K. *J. Phys. Chem.* **1990**, *94*, 4155.
(8) Okada, S.; Tezaki, A.; Miyoshi, A.; Matsui, H. *J. Chem. Phys.* **1994**, *101*, 9582.
(9) Hack, W.; Wagner, H. Gg.; Zasypkin, A. *Ber. Bunsen-Ges. Phys. Chem.* **1994**, *98*, 156.
(10) Yamasaki, K.; Okada, S.; Koshi, M.; Matsui, H. *J. Chem. Phys.* **1991**, *95*, 5087.
(11) Fueno, T.; Fukuda, M.; Yokoyama, K. *Chem. Phys.* **1988**, *124*, 265.
(12) Yokoyama, K.; Kitaike, H.; Fueno, T. *Bull. Chem. Soc. Jpn.* **1991**, *64*, 1731.
(13) Yokoyama, K.; Sakane, Y.; Fueno, T. *Bull. Chem. Soc. Jpn.* **1991**, *64*, 1738.
(14) Quandt, R. W.; Hershberger, J. F. *J. Phys. Chem.* **1995**, *99*, 16939.
(15) Durant, J. L., Jr. *J. Phys. Chem.* **1994**, *98*, 518.
(16) Mertens, J. D.; Chang, A. Y.; Hanson, R. K.; Bowman, C. T. *Int. J. Chem. Kinet.* **1991**, *23*, 173.
(17) Römming, H.-J.; Wagner, H. Gg. *26th Symp. (Int.) on Combustion*; The Combustion Institute, Baltimore, MD, 1996; Vol. 1, p 559.
(18) Patel-Misra, D.; Dagdigian, P. J. *J. Phys. Chem.* **1992**, *96*, 3232.
(19) Marshall, P.; Fontijn, A.; Melius, C. F. *J. Chem. Phys.* **1987**, *86*, 5540.
(20) Boehmer, E.; Shin, S. K.; Chen, Y.; Wittig, C. *J. Chem. Phys.* **1992**, *97*, 2536 and references therein.
(21) Brouard, M.; Burak, I.; Gatenby, S. D.; Hart, D.; Minayev, D. *J. Chem. Phys.* **1999**, *110*, 11335.
(22) Marshall, P.; Ko, T.; Fontijn, A. *J. Phys. Chem.* **1989**, *93*, 1922.
(23) Bozzelli, J. W.; Dean, A. M. *Int. J. Chem. Kinet.* **1995**, *27*, 1097.
(24) Hayhurst, A. N.; Hutchinson, E. M. *Combust. Flame* **1998**, *114*, 274.
(25) Walch, S. P. *J. Chem. Phys.* **1993**, *98*, 1170.
(26) Kristyan, S.; Lin, M. C. *Chem Phys. Lett.* **1998**, *297*, 200.
(27) Bradley, K. S.; McCabe, P.; Schatz, G. C.; Walch, S. P. *J. Chem. Phys.* **1995**, *102*, 6696.

(28) Simonson, M.; Bradley, K. S.; Schatz, G. C. *Chem. Phys. Lett.* **1995**, *244*, 19−26.
(29) Szichman, H.; Baer, M. *J. Chem. Phys.* **1996**, *105*, 10380.
(30) Laursen, S. L.; Grace, J. E., Jr.; DeKock, R. L.; Spronk, S. *J. Am. Chem. Soc.* **1998**, *120*, 12583 and references therein.
(31) Jacox, M. E. Vibrational and Electronic Energy Levels of Small Polyatomic Transient Molecules. In *NIST Chemistry WebBook*; Mallard, W. G.; Linstrom, P. J., Eds.; NIST Standard Reference Database 69; National Institute of Standards and Technology: Gaithersburg, MD, November 1998 (http://webbook.nist.gov).
(32) Kometer, R.; Legay, F.; Legay-Sommaire, N.; Schwentner, N. *J. Chem. Phys.* **1994**, *100*, 8737.
(33) Legay, F.; Legay-Sommaire, N. *J. Chem. Phys.* **1995**, *102*, 7798.
(34) Shimanouchi, T. *Tables of Molecular Vibrational Frequencies, Consolidated Volume I*; NSRDS−NBS 39, 1972.
(35) Shimanouchi, T. Tables of Molecular Vibrational Frequencies, Consolidated Volume II. *J. Phys. Chem.* **1977**, *6*, 993.
(36) McCarty, M., Jr.; Robinson, G. W. *J. Am. Chem. Soc.* **1959**, *81*, 4472.
(37) Bondybey, V. E.; Brus, L. E. *J. Chem. Phys.* **1975**, *63*, 794.
(38) Blindauer, C.; van Riesenbeck, N.; Seranski, K.; Winter, M.; Becker, A. C.; Schurath, U. *Chem. Phys.* **1991**, *150*, 93.
(39) Ramsthaler-Sommer, A.; Eberhardt, K. E.; Schurath, U. *J. Chem. Phys.* **1986**, *85*, 3760.
(40) Mielke, Z.; Latajka, Z.; Kolodzief, J.; Tokhadze, K. G. *J. Phys. Chem.* **1996**, *100*, 11610.
(41) Withnall, R.; Andrews, L. *J. Phys. Chem.* **1988**, *92*, 2155.
(42) Baronavski, A. P.; Miller, R. G.; McDonald, J. R. *Chem. Phys.* **1978**, *30*, 119.
(43) Gericke, K.-H.; Lock, M.; Comes, F. J. *Chem. Phys. Lett.* **1991**, *186*, 427.
(44) Haas, T.; Gericke, K.-H.; Maul, C.; Comes, F. J. *Chem. Phys. Lett.* **1993**, *202*, 108.
(45) Mélen, F.; Herman, M. *J. Phys. Chem. Ref. Data* **1992**, *21*, 831.
(46) Hetzler, J. R.; Casassa, M. P.; King, D. S. *J. Phys. Chem.* **1991**, *95*, 8086.
(47) Cheng, B.-M.; Lee, J.-W.; Lee, Y.-P. *J. Phys. Chem.* **1991**, *95*, 2814.
(48) Harrison, J. A.; Maclagan, R. *J. Chem. Soc., Faraday Trans.* **1990**, *86*, 3519.
(49) Herzberg, G. *Molecular Spectra and Molecular Structure*, 2nd ed. (reprinted); Krieger Publishing Co.: Malabar, FL, 1991; Vol. II.
(50) Thompson, W. E.; Jacox, M. E. *J. Chem. Phys.* **1999**, *111*, 4487.
(51) Feld, J.; Kunttu, H.; Apkarian, V. A. *J. Chem. Phys.* **1990**, *93*, 1009.
(52) Danilychev, A. V.; Apkarian, V. A. *J. Chem. Phys.* **1993**, *99*, 8617.
(53) Benderskii, A. V.; Wight, C. A. *J. Chem. Phys.* **1996**, *104*, 85.
(54) Benderskii, A. V.; Wight, C. A. *J. Chem. Phys.* **1994**, *101*, 292.
(55) Pettersson, M.; Lundell, J.; Räsänen, M. *J. Chem. Phys.* **1995**, *103*, 205.
(56) Feldman, V. I.; Sukhov, F. F. *Chem. Phys. Lett.* **1996**, *255*, 425.
(57) Laursen, S. L.; Olson, R.; Grace, J. E., Jr. Unpublished results.
(58) Chackerian, C., Jr.; Guelachvili, G.; López-Piñeiro, A.; Tipping, R. H. *J. Chem. Phys.* **1989**, *90*, 641.
(59) Collins, S. T.; Pimentel, G. C. *J. Phys. Chem.* **1984**, *88*, 4258.
(60) Laursen, S. L.; Pimentel, G. C. *J. Phys. Chem.* **1989**, *93*, 2328.
(61) Singmaster, K. A.; Pimentel, G. C. *J. Mol. Struct.* **1989**, *194*, 215.
(62) Laursen, S. L.; Pimentel, G. C. *J. Phys. Chem.* **1990**, *94*, 8175.
(63) Baldeschwieler, J. D.; Pimentel, G. C. *J. Chem. Phys.* **1960**, *33*, 1008.
(64) Kawai, J.; Tsunashima, S.; Sato, S. *Chem. Lett.* **1983**, 823.
(65) Milligan, D. E.; Jacox, M. E. *J. Chem. Phys.* **1964**, *41*, 2838.
(66) Sudhakar, P. V.; Lammertsma, K. *J. Am. Chem. Soc.* **1991**, *113*, 5219.
(67) Pehkonen, S.; Pettersson, M.; Lundell, J.; Khriachtchev, L.; Räsänen, M. *J. Phys. Chem. A* **1998**, *102*, 7643.
(68) DeMore, W. B., et al. *Chemical Kinetics and Photochemical Data for Use in Stratospheric Modeling*; NASA Evaluation No. 12 (JPL 97-4); Jet Propulsion Laboratory: Pasadena, CA, 1997.
(69) Linder, D. P.; Duan, X.; Page, M. *J. Chem. Phys.* **1996**, *104*, 6298.